Wheat-Gluten-Based Natural Polymer Nanoparticle Composites

Xiaoqing Zhang,* My Dieu Do, Katherine Dean, Pam Hoobin, and Iko M. Burgar

Commonwealth Scientific and Industrial Research Organization Manufacturing & Materials Technology, Private Bag 33, Clayton South MDC, Clayton South, Victoria 3169, Australia

Received September 28, 2006; Revised Manuscript Received November 8, 2006

A series of wheat-gluten-based nanocomposites were produced by dispersing Cloisite-30B nanoclay particles into plasticized wheat gluten systems under thermal processing conditions. The exfoliation of the nanoparticles as confirmed by wide-angle X-ray diffraction and transmission electron microscopy has resulted in significant enhancement of the mechanical properties for both deamidated proteins and vital gluten systems under 50% relative humidity (RH). Such strength improvement was also pronounced for wheat gluten (WG) systems under a high humidity condition (RH = 85%). A similar level of further strength enhancement was obtained for the WG systems that had been strengthened by blending with poly(vinyl alcohol) (PVA) and cross-linking with glyoxal. Although the nanoclay modifier, a quaternary ammonium, caused an additional plasticization to the materials, the interactions between the gluten matrix and the nanoparticles were predominant in all of these nanocomposites. A solid-state NMR study indicated that the polymer matrix in all of these nanocomposites displayed a wide distribution of chain mobilities at a molecular level (less than 1 nm). The interactions between the nanoparticles and the natural polymer matrix resulted in motional restriction for all components in the mobile phases including lipid, plasticizers, and plasticized components, although no significant influence from the nanoparticles was obtained in the mobility of the rigid phases (unplasticized components). On a scale of 20−30 nm, the deamidated protein systems tended to be homogeneous. The small domain size of the matrix resulted in modifications of the spin−lattice relaxation of these systems via spin diffusion. The residual starch seemed to remain in a relatively larger domain size in WG systems. The nanoparticles could enhance the miscibility between the starch and the other components in the WG nanocomposite, but such miscibility enhancement did not occur in the WG/PVA blend and the cross-linked system. These polymer matrixes were still heterogeneous on a scale of 20−30 nm.

1. Introduction

Development of renewable polymer materials from agriculture feedstocks has become a great challenge for material scientists due to increasing environmental concerns and diminishing petrochemical resources. Wheat gluten is one of the most important natural polymer resources due to its good viscoelastic properties, strong tensile strength, excellent gas barrier properties, low price, and constant quality with large-scale availability. Thermal processing is an efficient method to produce polymer materials; however, it is normally difficult to achieve for wheat gluten due to strong inter- and intramolecular interactions in conjunction with some extent of cross-linking among the protein macromolecules. A large amount of plasticizers is usually required in the process to reduce the strong inter-/intramolecular interactions and increase the mobility of the protein chains for reaching sufficient flexibility and extensibility of the materials.[1−8] Such plasticization significantly weakens the strength of the materials;[9−12] therefore, enhancement of the mechanical performance of plasticized wheat-gluten-based polymer materials plays a key role in extending the application of the materials.

Polymer/layered clay nanocomposites have attracted great interest from academic research and industries because significant improvement in many aspects of material performance can be obtained with a very low dosing amount of nanoparticles.[13−16] The main reason for such property improvement as compared to pure polymers or conventional composites (micro- or macrocomposites) is due to the significantly strengthened interfacial interactions between the polymer matrix and the nanoparticles (layer thickness on the order of 1−2 nm, diameter of 30−2000 nm) when such particles are well dispersed in the polymer matrix. Layered silicates such as montmorillonite, hectorite, and saponite are frequently used. Isomorphic substitutions in these layered clay sheets lead to a net negative charge necessitating the presence of cationic counterions in the intersheet region or gallery spacing. These counterions are usually exchanged with organic alkyl ammonium modifiers that would enhance the exfoliation in a polymer matrix.[13,17] Generally two types of polymer/layered clay nanocomposites are achievable and described on the basis of the particle dispersion, intercalated and exfoliated nanocomposites,[14] although a flocculated model was also mentioned.[18] The methodology also has been used to thermally process natural polymers such as starch and soy proteins.[19−23] Those fully or partially exfoliated nanocomposites achieved a remarkable improvement in tensile strength, stiffness, toughness, modulus, and barrier properties. Ultrasonic energy was also applied to promote the intercalation and exfoliation of unmodified montmorillonite clays when melt blending nanoparticles with biodegradable polymers.[22]

The focus of this work was to disperse a commercially available clay nanoparticle into plasticized wheat gluten/proteins to form nanocomposites and then to examine the enhancement of mechanical performance and the changes in phase structures of the materials. Alkyl-ammonium-modified montmorillonite clay (Cloisite-30B)[24] was used as the nanoparticle. The alkyl ammononium groups in the layered clay particles can improve the wetting characteristics of the polar protein chains, which

* Author to whom correspondence should be addressed. Phone: +63 95452653. Fax: +613 95441128. E-mail: Xiaoqing.Zhang@csiro.au.

10.1021/bm060929x CCC: $37.00
Published on Web 01/19/2007

Scheme 1. Organic Compound Used for Nanoclay Modification

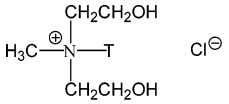

T = Tallow (~65% C18, 30% C16, 5% C14)

should benefit the exfoliation of the nanoparticles in wheat proteins. Several systems were studied including deamidated wheat proteins, vital wheat gluten, wheat gluten/poly(vinyl alcohol) (PVA) blend, and the wheat gluten/PVA blend cross-linked by glyoxal. Wide-angle X-ray diffraction (WAXD) and transmission electron microscopy (TEM) were applied to examine the intercalation or exfoliation of the nanoparticles in the nanocomposites. Dynamic mechanical analysis (DMA) was used to characterize the mechanical properties in conjunction with thermal behaviors. The influence of the nanoparticles on the molecular motions of each component in the proteins and phase structures of the whole nanocomposites were investigated by broad-line and high-resolution solid-state NMR techniques. The structural information obtained from the solid-state NMR study was correlated with the mechanical properties thus providing an inside understanding of the performance of the nanocomposites.

2. Materials and Methods

2.1. Materials. All raw wheat gluten/proteins samples were supplied by Manildra Group Australia. Raw wheat gluten (WG) vital contained ~80% proteins, 15% residual starch, 4% lipid, and ~1% fibers and other impurities on a dry basis. Deamidated wheat proteins (WPs) contained over 90% proteins, 5% lipid, and a small amount of residual starch (~3%) with other minor amounts of impurities. The deamidation was conducted under a mild alkaline condition resulting in 10−15% (WP-1) or 30−35% (WP-2) of the $-CONH_2$ side chains being broken leaving $-COO^-$ as end groups. The natural moisture content was ~12% for all three samples. Poly(vinyl alcohol) (PVA, Elvanol 71-30, fully hydrolyzed, fine powders) was obtained from DuPont and used as received. Glycerol was purchased from Aldrich while Cloisite-30B nanoparticles (C-30B), a natural montmorillonite modified with methyl tallow bis-2-hydroxyethyl quaternary ammonium chloride (Scheme 1),[24] was supplied by Southern Clay Products, Inc.

Plasticized WP-1, WP-2, or WG-1 samples were prepared using water (12%) and glycerol (15%) as plasticizers with pH = 4.0 as adjusted by acetic acid. A small amount of Na_2SO_3 (0.3 wt % to WP or WG) was added into all systems to dissociate the disulfide bonding within the protein chains to achieve efficient mixing between proteins and additives. Each sample with a designed formulation was mixed with a high-speed mixer operated at a speed of 3000 rpm for 1 min, left overnight, and then thermally mixed at an optimum condition (90−95 °C for 5 min at a speed of 100 rpm) in a Banbury mixer, and finally compression-molded at 130 °C for 5 min using a heating press with a pressure of 12 tons. The sample size was 145 mm × 145 mm with a thickness of 1.0 ± 0.1 mm.

WG/PVA (90:10) blend (WG-2) was prepared under the same procedures for preparing WG-1 but with the addition of 10 wt % of PVA (relative to dry WG/PVA) fine powder to the formulation. Approximately 1 wt % of glyoxal (relative to WG) was added into the plasticizer phase when preparing the cross-linked WG/PVA (90:10) blend (WG-3), and the same mixing and molding procedure was followed as for all samples.

For preparation of nanocomposite samples (WP-1N, WP-2N, WG-1N, WG-2N, and WG-3N), a 3 wt % amount of C-30B (relative to the wheat proteins or the WG/PVA blend) was dispersed into the plasticizer phase for each sample under a high shearing condition (4000 rpm for 10 min) to achieve a homogeneous dispersion. The plasticizer/C-30B was then mixed into the WP or WG materials, and the nanocomposites were processed using the same procedure as those without C-30B. All samples were conditioned under either a standard humidity condition (relative humidity (RH) of 50%) or a high humidity condition (RH = 85%) for a week, and then the moisture content of each sample (~12% for RH = 50% and ~21−22% for RH = 85%) was measured by drying the sample at 105 °C for 24 h. The total amount of plasticizer (water, glycerol, and acetic acid) in each sample is listed in Table 1, assuming only moisture content was changed during the thermal processing and conditioning.

2.2. Instrumentation. After the samples were conditioned at either relative humidity at room temperature for a week, the tensile strengths of these sheet samples were measured at room temperature, RH = 50%, on an Instron 5566P with a cross-head speed of 50 mm/min. The samples after conditioning were sealed in polyethylene bags when moving from the conditioning tank to the testing room, and the testing was conducted immediately. The data for each sample were obtained from an average of testing seven dog-bone-shaped specimens with an effective length of 30 mm and width of 6 mm.

The WAXD measurements were conducted on a Bruker D8 diffractometer operating at 40 kV, 40 mA, Cu Kα radiation monochromatized with a graphite sample monochromator. The diffractogram was recorded for 2θ angles from 2° to 25°.

Samples for TEM measurements were initially cross-linked with osmium tetroxide (OsO_4) prior to embedding in epoxy resins. The samples were then agitated in uncured epoxy resins for 24 h to encourage absorption of the resin into the samples followed by curing at 60 °C for 24 h. The 70−90 nm sections of the samples were microtomed at room temperature using an Ultracut E microtome at a cutting speed of 0.05 mm/s. A JEOL 100S transmission electron microscope was used at 100 keV with a magnification from 25 000× to 100 000×.

DMA experiments were conducted on a Perkin-Elmer Pyris Diamond dynamic mechanical analyzer in dual cantilever bending mode at a frequency of 1 Hz. The temperature range was set at −100 to 150 °C with a heating rate of 2 °C/min. The storage modulus (E'), the loss modulus (E''), and tan δ (E''/E') were recorded as a function of temperature throughout the experiment.

Broad-line pulse solid-state ^{1}H NMR was carried out on a Bruker Minispec PC 120 spectrometer at 20 MHz maintained at 40 °C for stable temperature control. The 90° pulse was 4.5 μs with a repetition of 2 s. The free induction decay (FID) signals of each sample were obtained by a solid−echo pulse sequence[25] and a Carr−Purcel−Meiboom−Gill (CPMG; 90°x−(t_1−180°y−t_1−echo)n) pulse sequence,[25] respectively. The 90°−90° pulse spacing in the solid−echo pulse sequence was 10 μs, and the dwell time was 1.25 μs. The 90°−180° pulse spacing (t_1) in the CPMG sequence was 50 μs, n was varied, and a total of 8 scans were used for each measurement. The whole FID of each sample was a combination of the data observed from solid−echo (time range of 0−0.15 ms) and from CPMG (time range of 0.4−8.0 ms) pulse sequences, and then a multidecay function was used to best fit the FID data with the IGOR program from Wave Metrics, Inc., as described in previous papers.[27,28]

High-resolution solid-state NMR experiments were conducted at room temperature using a Varian Unity plus spectrometer at resonance frequencies of 75 MHz for ^{13}C and 300 MHz for ^{1}H. ^{13}C NMR spectra were observed under cross-polarization (CP), magic angle spinning (MAS), and high power dipolar decoupling (DD) techniques. The 90° pulse was 4.5 μs for ^{1}H and ^{13}C, the radio frequency (rf) strength for spin-locking was 56 kHz, and the spinning rate of MAS was approximately 7−8 kHz. A contact time of 1.0 ms was used for measuring all CP/MAS spectra with a repetition time of 2 s. The chemical shifts of the ^{13}C spectra were determined by taking the carbonyl carbon of solid glycine (176.03 ppm) as an external reference standard. ^{1}H MAS NMR spectra were obtained with the same MAS rates, and tetramethylsilane (TMS) was used as an external chemical shift reference.

Table 1. Mechanical Properties of WP and WG Systems[a]

	plasticizers (%)	tensile strength (MPa)		elongation at breakage (%)		Young's modulus (MPa)	
samples	RH = 50%	RH = 50%	RH = 85%	RH = 50%	RH = 85%	RH = 50%	RH = 85%
WP-1	29	5.8	3.2	184	210	66.9	59.2
WP-1N	28	7.8	3.1	141	139	98.9	63.4
WP-2	29	5.9	3.1	154	223	74.7	52.9
WP-2N	28	8.8	3.8	83	147	85.9	69.7
WG-1	29	5.8	3.0	106	239	65.4	43.4
WG-1N	28	9.0	4.6	78	98	91.8	62.6
WG-2	26	10.8	4.9	74	128	100.8	62.0
WG-2N	25	12.6	6.4	68	89	105.2	68.7
WG-3	27	10.5	5.2	104	128	93.1	62.3
WG-3N	27	13.9	6.5	58	63	106.2	73.9

[a] The error bar is ~5−7%.

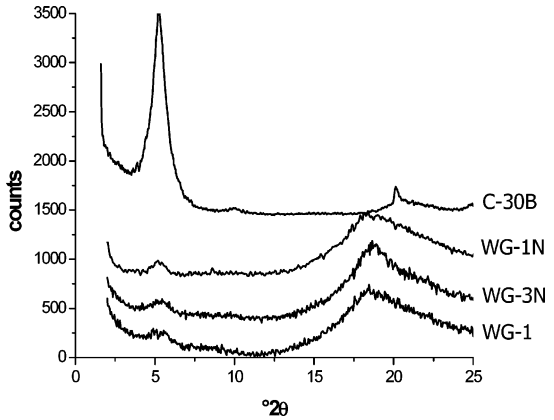

Figure 1. WAXD diffractograms of WG-1, WG-1N, WG-3N, and Cloisite-30B (C-30B).

^{1}H spin−spin (T_2) and spin−lattice (T_1) relaxation times under high-resolution conditions (MAS) were measured through the decay of ^{1}H intensities in MAS spectra observed by the CPMG pulse sequence (t_1 of 40 μs) or the inversion recovery (180°−τ−90°) pulse sequences,[25] respectively, with a repetition time of 2 s and a 90° pulse length of 2.5 μs. The ^{1}H T_2 or T_1 data were also measured through the change of ^{13}C magnetization prepared by CP with varied CP delay times (16 points between 2 and 100 μs) or via a pulse sequence to transfer the ^{1}H magnetization to ^{13}C through CP after the inversion recovery in the ^{1}H channel (with 16 varied τ values over a range from 0.001 to 5 s.) as reported previously.[26,27]

3. Results and Discussion

The structure of polymer/clay nanocomposites can be typically elucidated by WAXD and TEM. Usually WAXD provides a convenient method to compare the interlayer spacing in the original clay to those in the nanocomposites. However, TEM allows a qualitative examination of dispersion of the nanoparticles and phase structures of the nanocomposites through direct visualization. Both techniques were applied to the wheat-protein-based nanocomposites, and typical results are shown in Figures 1 and 2. The WAXD diffractograms of pure C-30B (Figure 1) displayed a strong peak at 5.2° (2θ) corresponding to an average interlayer clay spacing of 17.5 Å, which is consistent with that reported in literature.[16] When the nanoparticles were dispersed in a series of WG systems (WG-1N and WG-3N in Figure 1), this peak was significantly reduced in intensity, and the diffractogram showed a similar pattern to that of WG without any C-30B (WG-1), indicating that sufficient exfoliation was achieved in these nanocomposites. The TEM images of WG-1N and WG-3N (Figure 2) confirmed the WAXD results, showing that single exfoliated silicates were the predominant structure in the nanocomposites. There were some smaller tactoids (3−5 particles), but no large agglomerates were visible in the systems.

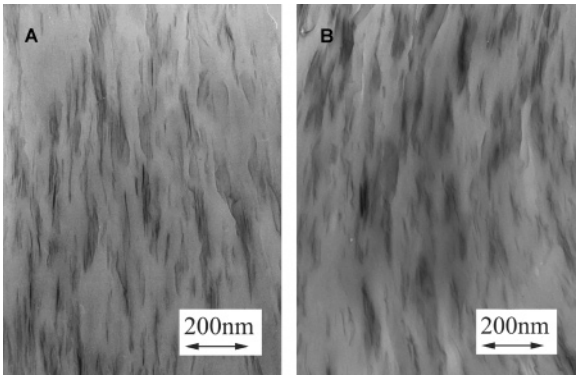

Figure 2. TEM images of (A) WG-1N and (B) WG-3N.

Such exfoliation of the nanoparticle composites resulted in significant improvement in mechanical strength. Table 1 lists the mechanical properties of a series of plasticized wheat protein materials and their nanocomposites measured after conditioning the samples under two RH conditions (50% and 85%) for 7 days. The plasticizer content was slightly lower in the nanocomposites due to the addition of nanoparticles to the total mass. Under RH = 50% (moisture content ~12%), most of the nanocomposites showed significant improvements in tensile strength and modulus as compared to their corresponding systems without nanoparticles. The elongation at breakage decreased but still remained at a sufficient level for flexibility of the composites. The nanoparticles were indeed effective at improving the mechanical properties of all wheat protein systems studied in the work, even for the WG-2 and WG-3 systems where the strength had been already enhanced by blending with PVA and further cross-linking.

Similar strength enhancement was also obtained after conditioning the nanocomposites under RH = 85% for 7 days (except for the WP-1N). However, the values of the tensile strength were around 50% of those under RH = 50% due to the increase of moisture content in the systems under the high humidity condition (now ~21−22%). In comparison to the values at RH = 50%, the modulus of the systems also decreased, and the elongation was increased in most cases as the additional moisture content would contribute to the plasticization of the materials. Most nanocomposite samples displayed a stronger modulus and short elongation as compared to the systems

Table 2. DMA Results for WP and WG Systems[a]

samples	tan $\delta - \beta$ (°C)	tan $\delta - \alpha_2$ (°C)	tan $\delta - \alpha_1$ (°C)	tan δ max (α_1)
WP-1	−50	26	91	0.489
WP-1N	−50	28	93	0.455
WP-2	−58	24	119	0.512
WP-2N	−55	22	108	0.481
WG-1	−55	31	104	0.463
WG-1N	−53	33	107	0.424
WG-2	−60	31	102	0.444
WG-2N	−60	32	104	0.409
WG-3	−60	32	105	0.405
WG-3N	−57	33	107	0.402

[a] The temperature error bar is ±1−2 °C.

without nanoparticles. Variation of moisture (plasticizer) content over a range did not influence the nanoparticles' effect to improve the mechanical properties of wheat protein systems.

DMA was also conducted for these wheat protein systems. The general DMA behavior of the systems was similar to those of plasticized wheat proteins,[6−8,27] and the results of WP, WG, and their nanocomposites are shown in Figures 3 and 4. As temperature increased, E' (storage modulus) decreased slowly and then dropped markedly at a typical temperature due to the glass transition of the systems. The onset of this E' decrease was taken as the start of the T_g transitions, while a strong tan δ peak was observed corresponding to the transitions. At a temperature range from −60 to −50 °C, a minor tan δ peak was obtained in conjunction with E' onset due to β-transitions of the systems.[6−8,27] The behavior did not vary significantly for all of the systems (Table 2), suggesting that the β-transitions were not influenced by the nanoparticles. Although a certain amount of water (~12%) was present in the systems, a transition due to ice melting was not observed at approximately 0 °C, indicating that the water molecules were strongly hydrogen-bonded with protein macromolecules and did not exist as free water as described in previous reports.[27]

Comparison of the DMA data of WP-1 and WP-2 with those of their nanocomposites (Figure 3) showed that E' of the nanocomposites became slightly lower for the nanocomposites at lower temperatures but remained at a relatively high level at high temperatures above the T_g. The E' values of WP-1 systems were always lower than those of WP-2 systems especially in the low-temperature range. The tan δ peaks due to T_g of all these systems were broad, but the peak became slightly narrower in the nanocomposites. The maximum of tan δ in WP-1N was significantly lower than that of WP-1, suggesting motional restriction, but the change between WP-2 and WP-2N was minimal. Only a minor variation was observed in the DMA patterns of WG-1, WG-2, and WG-3, but there was a significant effect from the nanoparticles, and the changes in the DMA curves are shown in Figure 4. The E' data in the low-temperature range were similar for all WG systems, but E' decreased earlier in the nanocomposites as the temperature increased (E' onset appeared at lower temperatures), suggesting their T_g transitions started at relatively lower temperatures. Best fitting the results of the tan δ curves suggested two T_g transitions (α-transitions) for all of the systems as listed in Table 2. The relatively weak peaks (tan $\delta - \alpha_2$) appearing at a lower temperature around 26−33 °C should be attributed to the T_g of the plasticized matrixes/phases. The T_g values are higher than those reported for plasticized soy proteins[30] due to the different moisture content (derived from different RH conditions) in the two systems. Although the dispersion of the nanoparticles caused

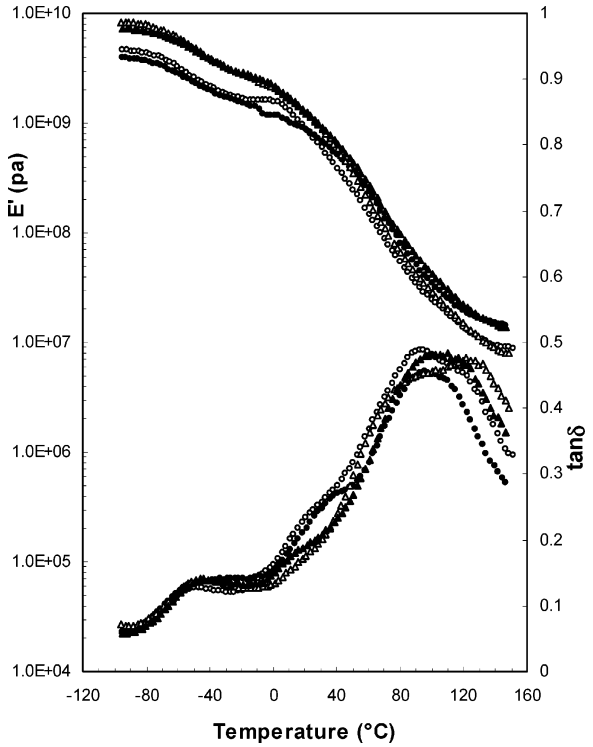

Figure 3. Storage modulus (E') and tan δ of WP-1 (○), WP-1N (●), WP-2 (△), and WP-2N (▲).

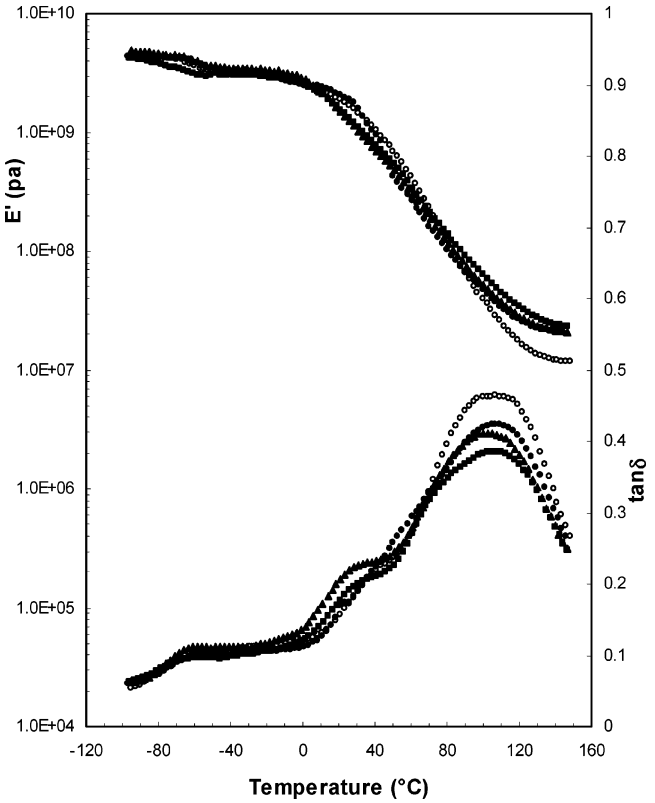

Figure 4. Storage modulus (E') and tan δ of WG-1 (○), WG-1N (●), WG-2N (▲), and WG-3N (■).

the T_g transition to start at lower temperatures for the matrix, it only broadened the tan $\delta - \alpha_2$ peaks but did not shift the maximum of these peaks significantly. The major tan δ peaks (tan $\delta - \alpha_1$) shifted slightly to higher temperatures when nanoparticles were used (except WP-2N), but the maximum values of the tan δ peaks were significantly reduced, being consistent with those found in soy protein/nanoclay systems.[23]

The E' values of the nanocomposites above T_g were always higher than those of the systems without nanoparticles. WG-3N displayed the highest E' value and lowest tan δ maximum above T_g, corresponding to the highest modulus and motional restriction due to a combination of blending, cross-linking, and interactions with nanoparticles.

Normally exfoliation of nanoparticles in a polymer matrix results in an increase in T_g due to interactions between the polymer chains and the nanoparticles.[18,21,22] The decrease in T_g of wheat proteins/C-30B nanocomposites is possibly due to the use of organics for modification of the nanoparticles. Approximately 30% methyl tallow bis-2-hydroxyethyl quaternary ammonium chloride (Scheme 1) was used as a modifier in C-30B, which could act as an efficient plasticizer (~1 wt % to the proteins) in the polymer matrix. Due to the hydrophilic nature of deamidated WP-1 and WP-2, the same amounts of water and glycerol could result in a more efficient plasticization in these systems as compared to those in WG systems.[8] Further introduction of a small amount of the quaternary ammonium might not display a significant additional plasticization for these WP systems. However, this amount of the alkyl quaternary ammonium (~1%) could show a more remarkable effect in plasticization of the WG systems. It seemed that the interactions with nanoparticles (motional restriction) and additional plasticization (mobility enhancement) were present simultaneously in the protein matrix. The lower E' of some nanocomposites might be due to the additional plasticization effect; however, the nanoparticles' effect became more pronounced above T_g for most of the nanocomposites. This resulted in motional restriction to the protein matrix and improvement of tensile strength and modulus in the nanocomposites in conjunction with a decrease in elongation. In these plasticized systems, the amount of plasticizers always plays a major role in their mechanical properties. At a critical level of plasticization, a small variation of effective plasticizers would modify the molecular motions of natural polymers significantly. The additional plasticization effect from the alkyl quaternary ammonium might play a negative role in achieving even higher strength enhancement in the nanocomposites; however, the modifier was necessary for an efficient exfoliation of the nanoparticles, which is fundamental for such strength improvement. The hydrophilic nature of WP-1 and WP-2 could result in stronger interactions with plasticizers as compared to that of WG (even with the same content of plasticizers) but weaker interactions with nanoparticles. This might play a certain role in inhibiting the strength improvement in WP-1N and WP-2N nanocomposites especially under a high humidity condition.

The broad tan δ peaks corresponding to T_g transitions of these nanocomposites obtained by DMA are due to the presence of a series of complicated phase structures in the systems such as the plasticized phase, the partially plasticized phase, and the nonplasticized phase in conjunction with their different interactions with nanoparticles. In addition, multiple components such as proteins, starch, lipids, polymer additives (PVA), and plasticizers coexist in the systems, and their interactions with the nanoparticles would also behave differently. The cross-linking also played a role in the WG-3 and WG-3N systems. In a series of our recent studies on thermally processed wheat-protein-based materials,[6−8,27−29] solid-state NMR techniques were applied to investigate the plasticizing, blending, and cross-linking effects on each component in wheat protein systems and intermolecular interactions among these different components in the whole materials. The same methodology was applied to the wheat-protein-based nanocomposites to examine the effects of nanoparticles on the molecular motions of these different components and phase structures of the whole materials from the molecular level to a scale of 20−30 nm.

Table 3. ^{1}H Spin−Spin Relaxation Time T_2 Values (μs) and Their Proportions (%) Obtained via Analysis of ^{1}H FID Signals*

samples	T_{2S}	A_{2S} (%)	T_{2M}	A_{2M} (%)	T_{2L}	A_{2L} (%)
WP-1	11.1	45	210	51	1030	4
WP-1N	10.8	42	182	47	966	11
WP-2	11.1	44	172	48	920	8
WP-2N	11.3	43	151	53	770	4
WG-1	11.1	46	103	29	980	25
WG-1N	11.3	45	65	36	619	19
WG-2	9.1	55	118	25	501	20
WG-2N	9.6	53	53	30	488	17
WG-3	9.7	56	109	28	751	16
WG-3N	10.4	55	59	37	539	8

*The error bar is ~3−5%.

^{1}H spin−spin relaxation (T_2) is sensitive to the mobility of polymers at molecular levels.[25] The analysis of FID data from a combination of the signals observed via solid−echo (sensitive to rigid components) and CPMG (sensitive to mobile components) pulse sequences would provide information about both the motion (T_2 value) and the proportion (the intensity of the T_2 component) of each phase component.[26] The ^{1}H T_2 values obtained by the same method for wheat-protein-based materials and their nanocomposites are summarized in Table 3. As in previous reports,[27−29] three components were indeed obtained for all samples after applying curve fitting, including a Gaussian decay with a short T_2 value (T_{2S}) and two exponential decays with longer T_2 values (T_{2M} and T_{2L}). The three phases were correlated to rigid, intermediate, and mobile phases, respectively. The chemical nature of the three phases was also examined previously[8,27] and is summarized below: The rigid T_{2S} phase mainly consists of unplasticized proteins and starch (especially in WG systems), the T_{2M} phase is due to plasticized proteins and starch, and the lipid remains in the T_{2L} phase. Plasticizers such as water and glycerol could be present in all three phases and interact with different components mainly via hydrogen-bonding interactions. Their distribution in the three phases depends on the nature of the plasticizers and the amount of plasticizers used. In the cases studied in this work, the plasticizers remained mainly in the intermediate and mobile phases.

The dispersion of nanoparticles into these plasticized protein systems caused a significant reduction in T_{2M} and T_{2L}, suggesting motional restriction in these mobile phases of nanocomposites. Note that T_{2M} and T_{2L} of the WG systems were reduced more significantly than those of WP-1 and WP-2, suggesting that the impact was stronger in the WG systems. Most of the phase proportions of the T_{2M} phases increased in the nanocomposites while those of T_{2L} decreased (except WP-1N). For the T_{2S} phases, no significant influence from the nanoparticles was observed; the T_2 values reflected a small increase while the T_{2S} proportions decreased slightly in the nanocomposites. These results seemed more relevant to the additional plasticization by the quaternary ammonium associated with the nanoparticles. Higher T_{2S} proportions obtained in the WG-2 and WG-3 systems were attributed to the blending with PVA (PVA mainly remained in the rigid phase[6]) and the cross-linking with glyoxal.[29] The high proportion of rigid phases in the WG systems would contribute to their higher tensile strengths and moduli but shorter elongations for these systems (Table 1). The

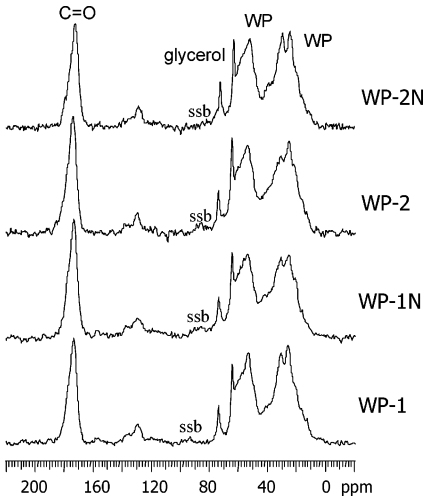

Figure 5. ^{13}C CP/MAS NMR spectra of WP-1, WP-2, and their nanocomposites WP-1N and WP-2N. Spinning side bands are designated by ssb.

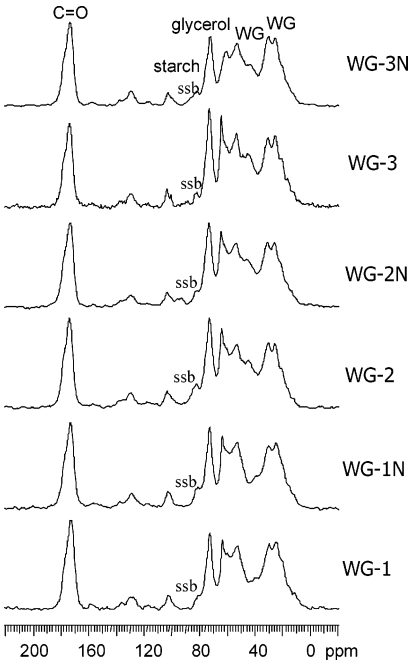

Figure 6. ^{13}C CP/MAS NMR spectra of WG-1, WG-2, WG-3, and their nanocomposites WG-1N, WG-2N, and WG-3N. Spinning side bands are designated by ssb.

nanoparticles showed a minor effect on the mobility of the rigid phase, and ^{1}H T_2 is not sensitive to the mobility variation in such rigid phases. Usually DMA provides motional information about polymer components over a scale of 20−100 nm while ^{1}H T_2 is very sensitive to local dipolar interactions at the molecular level (a scale below 1 nm). The two methodologies provide information about motional dynamics of a material on different scales. The result indicates that phase mobility and compositions of the wheat-protein-based nanocomposites had a direct relationship with their mechanical performance. Further detailed information about the behavior of each component with the nanoparticles can be examined by using high-resolution solid-state NMR techniques.

The CP/MAS ^{13}C NMR spectra of WP, WG, and their nanocomposites are shown in Figures 5 and 6. The CP/MAS method is sensitive to the rigid materials where strong dipolar interactions in the system allow polarization transfer from protons to nearby carbons, thus efficiently enhancing the carbon

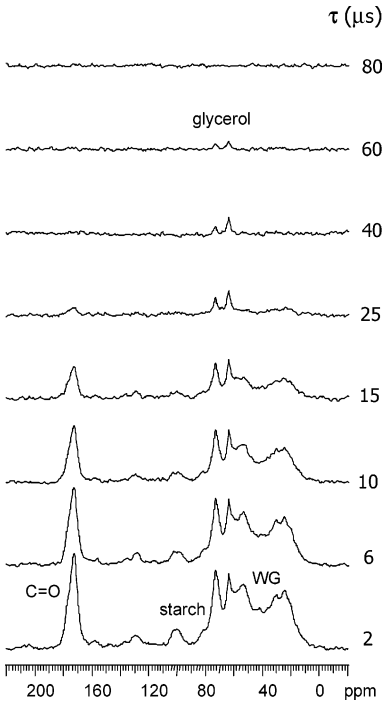

Figure 7. ^{13}C CP/MAS NMR spectra of WG-2N measured with varied CP delay times (τ) where the intensity decay follows ^{1}H T_2 decay.

intensities. The assignments of the systems have been reported previously; the major protein resonances at 173, 54, and 30−15 ppm are attributed to the carbonyl, C-α, C-β, and C-γ carbons of proteins, respectively, while minor resonances in the spectrum at 157, 138, 129, and 116 ppm are due to Arg, Tyr, and Phe.[31−33] The resonances of residual starch (more significant in the WG systems (Figure 6) were obtained at 103, 83, and 74 ppm (C-1, C-4, and C-2, 3, and 5 of starch) while the C-6 peak at 62 ppm overlapped with the resonances of the proteins. Two sharp peaks at 64 and 74 ppm are due to the plasticizer glycerol in all cases. The ^{13}C NMR signals of PVA[6,34−37] appear in the range of 40−80 ppm, which overlaps with the resonances of starch and proteins. The low intensity (low content in the systems) also made it difficult for the signals to be distinguished. For all of the WP and WG systems, the dispersion of the nanoparticles did not change the pattern of the spectra significantly, which is consistent with that obtained from the ^{1}H T_2 study where there was no significant effect from nanoparticles on the rigid components in the nanocomposites.

Examination of ^{1}H T_2 measured via high-resolution solid-state NMR techniques can provide the motional information about each component in such multicomponent systems. The ^{13}C CP/MAS NMR spectra of WG-2N observed with varied CP delay times (τ) are shown in Figure 7. After the 90° pulse in the proton channel, the proton resonances decreased their intensities following ^{1}H T_2 decay.[26,27] Because the intensities of the ^{13}C resonances were enhanced by proton magnetization through energy exchange during CP time, the intensity of each ^{13}C resonance versus CP delay time reflected the ^{1}H T_2 decay of the protons in the rigid phase that was capable of transfering their magnetization to the ^{13}C resonance. Mainly the chemically bonded protons or those located close enough to the carbon in the structure can exchange energy with the ^{13}C resonance. Most of the resonances decayed rapidly as τ time increased, and when τ reached 30 μs, the only signals that remained were glycerol at 73 and 64 ppm. The behaviors of the other WP and WG systems were similar, suggesting that the rigid phases (T_{2S}) in the nanocomposites were still the same as those without

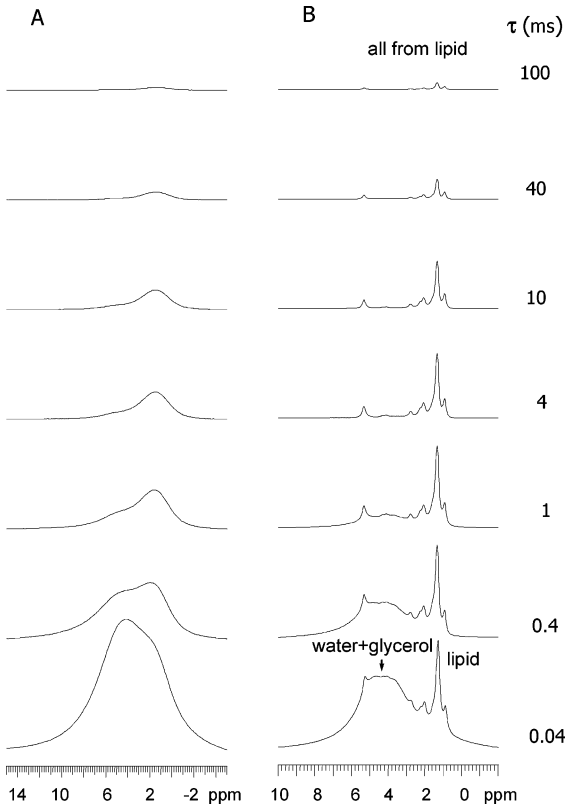

Figure 8. ^{1}H NMR spectra of WG-1N observed by the CPMG pulse sequence (A) without MAS and (B) with MAS under varied τ delay times.

nanoparticles. The PVA also remained in the rigid phases. The observation of glycerol signals via CP methods further indicated the strong hydrogen-bonding association between glycerol and the protein matrix even in the rigid phases. Certainly, the majority of glycerol still remained in the mobile phases.

The existence of mobile components in the system has also made it possible to observe high-resolution solid-state ^{1}H NMR spectra by the MAS technique under a low spinning rate at approximately 7 kHz. Only mobile components such as lipid and plasticizers can be obtained by this method while the rigid phases would be missed as a broad baseline. Figure 8 shows the ^{1}H spectra of a nanocomposite WG-1N observed by the CPMG pulse sequence using typical τ times at which the *n*th echo appeared under (A) static and (B) MAS conditions. Under static conditions (A), mainly two broad peaks with a great extent of overlapping were detected at approximately 4.0 and 1.5 ppm corresponding to plasticizers (water and glycerol) and lipids, respectively. Application of MAS resulted in significant line width narrowing, and many narrow resonances were detected as shown in Figure 8B. These narrow peaks at 0.9, 1.3, 2.0, and 5.2 ppm were all assigned to lipid resonances[38] while the broad peak at approximately 4.0 ppm was due to water and glycerol. The minor amount of resonances for proteins (if existing) might overlap with these strong resonances. As the time τ increased, the intensity of the water/glycerol peak (4.0 ppm) decayed much faster than these lipid resonances under both static and MAS conditions, indicating that lipid was more mobile.

Table 4 summarizes the ^{1}H T_2 data for the systems measured via ^{1}H NMR spectra under MAS and static conditions. The T_2 value for the lipids was always longer than those of the plasticizers, and the application of MAS did increase the T_2 values of both plasticizers and lipids. Different lipid resonances also displayed different T_2 values; the chain $-CH_2-$ (1.3 ppm) and end group $-CH_3$ (0.9 ppm) resonances always had a longer T_2 value while the resonances of $-CH_2-COO-$ (2.1 ppm) and olefinic protons (5.3 ppm) had shorter T_2 values, but the T_2 data for the plasticizers at 4.0 ppm were always the shortest in all of the systems. The MAS effect to these T_2 data has been discussed previously and could be attributed to the different line width broadening for lipid and water/glycerol.[38−40] Such behavior remained in the nanocomposites; however, the ^{1}H T_2 values of all of these mobile components were significantly reduced as compared to those without nanoparticles. The effect was more pronounced on lipids possibly because the chemical nature of tallow in the quaternary ammonium was similar to that of lipids and could interact with lipids intimately, thus causing strong interactions between lipids and nanoparticles.

Table 4. ^{1}H Spin−Spin Relaxation Time T_2 Values (ms) Obtained via ^{1}H Spectra[a]

	MAS					no MAS	
samples	5.2 ppm	4.0 ppm	2.1 ppm	1.3 ppm	0.9 ppm	4.0 ppm	1.5 ppm
WP-1	0.64	0.55	1.6	11.7	8.8	0.42	0.97
WP-1N	0.58	0.54	1.7	7.7	6.8	0.41	0.66
WP-2	0.63	0.58	0.93	7.2	6.0	0.43	0.71
WP-2N	0.43	0.43	0.73	4.6	3.1	0.39	0.48
WG-1	0.82	0.62	3.7	25.9	18.7	0.45	0.85
WG-1N	0.61	0.47	3.0	13.4	10.5	0.43	0.68
WG-2	1.10	0.43	10.8	27.9	15.3	0.40	0.85
WG-2N	1.13	0.43	7.16	16.8	13.1	0.39	0.71
WG-3	1.91	0.42	11.1	25.2	20.1	0.39	0.82
WG-3N	1.00	0.40	5.98	14.0	9.57	0.38	0.63

*The error bar is ∼5%.

Table 5. ^{1}H Spin−Lattice Relaxation Time T_1 Values (s)[a]

	via ^{13}C CP/MAS spectra			via ^{1}H MAS spectra	
samples	proteins	starch	glycerol	lipid	water/glycerol
WP-1	0.35		0.36	0.39	0.37
WP-1N	0.21		0.21	0.26	0.20
WP-2	0.30		0.24	0.30	0.26
WP-2N	0.18		0.21	0.20	0.19
WG-1	0.63	0.82	0.64	0.59	0.65
WG-1N	0.23	0.38	0.28	0.35	0.29
WG-2	0.42	0.78	0.38	0.37	0.39
WG-2N	0.22	0.72	0.23	0.33	0.24
WG-3	0.37	0.88	0.37	0.40	0.36
WG-3N	0.19	0.71	0.21	0.31	0.23

*The error bar is ∼10% for the starch component and ∼3−5% for the other components.

The study of ^{1}H spin−lattice T_1 relaxations of each component in a multicomponent system can explore not only the molecular motions in the megahertz range but also the homo- or heterogeneity of the whole systems on a scale of ca. 20−30 nm, which is the effective spin-diffusion length during the T_1 relaxation times.[41−45] ^{1}H T_1 data for the wheat-protein-based materials or nanocomposites were observed either via ^{13}C resonances through CP/MAS (mainly the rigid phases/components) or via their ^{1}H MAS spectra (the mobile components/phases) and are listed in Table 5. The repetition time of 2 s used for T_1 measurements was a little short for longer T_1 components such as starch; however the error should not affect the trends of the relaxation behavior for each component in the systems. The comparison of ^{1}H T_1 data observed by the two methods should therefore provide the strength of dipolar interactions among different components or phases with different chemical natures or molecular mobilities, thus exploring the

nanoparticle effect on the molecular motions and homogeneity or heterogeneity of the whole system on a scale of 20−30 nm.

The ^{1}H T_1 data for protein components observed at 174 and 30−25 ppm via ^{13}C CP/MAS spectra were quite similar in most of samples, indicating a strong spin-diffusion interaction among the components; thus, their averaged values are shown in Table 5 as the T_1 value of the protein component in each sample. The T_1 data detected at 103 ppm reflected the behavior of the starch component, while those of glycerol were detected from the narrow line at 64 ppm. For those obtained via ^{1}H MAS spectra, the T_1 data for the lipids were measured at 1.3 ppm (the $-CH_2-$) while those of the plasticizers were detected at 4.0 ppm.

In WP systems that contained a low level of residual starch, the ^{1}H T_1 values observed for different components via different methods tended to be similar, implying that the systems could be relatively homogeneous at a scale of 20−30 nm. Applying nanoparticles significantly reduced the T_1 values for all components to a similar level, indicating that strong spin diffusion had averaged out the effects of modification in phase structures and molecular motions of the nanocomposites. However, the situation became different in WG systems. The T_1 value observed for the starch component was quite different from those of proteins, lipids, and plasticizers, indicating that the starch was not mixed intimately with the other components at a scale of 20−30 nm. When nanoparticles were introduced into the systems, the T_1 data decreased for all of the cases, being consistent with the modification of nanoparticles, the same as in the WP systems. It seemed that the nanoparticles also enhanced the miscibility between starch and other components in WG-1N; the T_1 data became much closer to each other for all of the components. However, when blending PVA and cross-linking were applied in the systems (WG-2N and WG-3N), such a miscibility enhancement effect disappeared; the T_1 value of the starch component did not decrease as much as that in WG-1N, although the nanoparticles still generated a T_1 decrease similar to those of all of the other components in the nanocomposites. The matrixes of WG-2N and WG-3N were heterogeneous at a scale of 20−30 nm. The presence of different phase structures at 20−30 nm could be the reason for multiple T_g transitions observed in DMA measurements.

4. Conclusions

Wheat-gluten-based nanocomposites were produced by dispersing Cloisite-30B nanoclay particles into a series of plasticized wheat gluten/protein systems through thermal processing. The exfoliation of the nanoparticles resulted in significant enhancement of mechanical properties at RH = 50% for all of the systems studied. Such an improvement was also pronounced for WG systems under a high humidity condition (RH = 85%). For the WG systems that had been strengthened by blending with PVA and cross-linking with glyoxal, a similar level of further strength enhancement was obtained. Although the nanoclay modifier, a quaternary ammonium, caused an additional plasticization to the wheat protein systems (causing the T_g transitions to start at relatively lower temperatures), the interactions between the protein matrix and the nanoparticles were still predominant in all of these nanocomposites. Solid-state NMR results indicated a wide distribution of molecular mobility through the matrix at a molecular level. The interactions between the nanoparticles and the natural polymers resulted in significant motional restriction for all of the components in the mobile phase including lipids, plasticizers, and plasticized phases while the mobility in the rigid phases (unplasticized components) was only slightly influenced by the nanoparticles. In the WP-based nanocomposites the matrix tended to be homogeneous on a scale of 20−30 nm, and the small domain size caused a modification of spin−lattice relaxation of the whole systems via spin diffusion. However, the domain size of the residual starch remained relatively larger in some of the WG systems. The nanoparticles enhanced the miscibility between the starch and the other components in WG-1N, but such miscibility enhancement did not occur in the WG/PVA blend and the cross-linked WG/PVA system where the polymer matrix was still heterogeneous on a scale of 20−30 nm. Such multiphase character with strong intermolecular interactions among different polymer components in the matrix should be favorable for advanced properties of the nanocomposites, as demonstrated in the improved mechanical performance of WG-2N and WG-3N nanocomposites.

References and Notes

(1) Ali, Y.; Ghorpade, V. M.; Hanna, M. A. *Ind. Crops Prod.* **1997**, *6*, 177−184.
(2) John, J.; Tang, J.; Bhattacharya, M. *Polymer* **1998**, *39*, 2883−2895.
(3) Redl, A.; Morel, M.; Bonicel, J.; Vergnes, B. *Cereal Chem.* **1999**, *76*, 361−370.
(4) Micard, V.; Morel, M.-H.; Bonicel, J.; Guilbert, S. *Polymer* **2001**, *42*, 477−485.
(5) Gallstedt, M.; Mattozzi, A.; Johansson, E.; Hedenqvist, M. S. *Biomacromolecules* **2004**, *5*, 2020−2028.
(6) Zhang, X.; Burgar, I.; Lourbakos, E.; Beh, H. *Polymer* **2004**, *45*, 3305−3312.
(7) Zhang, X.; Do, M.; Lourbakos, E. *Polym. Prepr. (Am. Chem. Soc., Div. Polym. Chem.)* **2005**, *46*, 321−322.
(8) Zhang, X.; Burgar, I.; Do, M.; Lourbakos, E. *Biomacromolecules* **2005**, *6*, 1661−1671.
(9) Pouplin, M.; Redl, A.; Gontard, N. *J. Agric. Food Chem.* **1999**, *47*, 538−543.
(10) Irissin-Mangata, J.; Bauduin, G.; Boutevin, B.; Gontard, N. *Eur. Polym. J.* **2001**, *37*, 1533−1541.
(11) Pommet. M.; Redl, A.; Morel, M. H.; Guilbert, S. *Polymer* **2003**, *44*, 115−122.
(12) Pommet, M.; Redl, A.; Guibert, S.; Morel, M.-M. *J. Cereal Sci.* **2005**, *42*, 81−91.
(13) Giannelis, E. P. *Appl. Organomet. Chem.* **1998**, *12*, 675−680.
(14) LeBaron, P. C.; Wang, Z.; Pinnavaia, T. J. *Appl. Clay Sci.* **1999**, *15*, 11−29.
(15) Schmidt, D.; Shah, D.; Giannelis, E. P. *Curr. Opin. Solid State Mater. Sci.* **2002**, *6*, 205−212.
(16) Fisher, H. *Mater. Sci. Eng., C* **2003**, *23*, 763−772.
(17) Bharadwaj, R. K.; Mehrabi, A. R.; Hamilton, C.; Trujillo, C.; Murga, M.; Fan, R.; Chavira, A.; Thompson, A. K. *Polymer* **2002**, *43*, 3699−3705.
(18) Ray, S. S.; Okamoto, K.; Okamoto, M. *Macromolecules* **2003**, *36*, 2355−2367.
(19) Park, H.-M.; Li, X.; Jin, C.-Z.; Park, C.-Y.; Cho, W.-J.; Ha, C.-S. *Macromol. Mater. Eng.* **2002**, *287*, 553−558.
(20) Park, H.-M.; Lee, X.-K.; Park, C.-Y.; Cho, W.-J.; Ha, C.-S. *J. Mater. Sci.* **2003**, *38*, 909−915.
(21) Wilhelm, H.-M.; Sierakowski, M.-R.; Souza, G. P.; Wypych, F. *Carbohydr. Polym.* **2003**, *52*, 101−110.
(22) Dean, K.; Yu, L. *Biodegradable Polymers for Industrial Applications*; Smith, R., Ed,; Woodhead Publishing: Cambridge, U. K., 2005; pp 289−309.
(23) Huang, X.; Netravali, A. N. *Biomacromolecules* **2006**, *7*, 2783−2789.
(24) Cloisite 30B Typical Physical Properties Bulletin. http://www.scprod-.com/product_bulletins/PB%20Cloisite%2030B.pdf.
(25) McBrierty, V.; Packer, K. *Nuclear Magnetic Resonance in Solid Polymers*; Cambridge University Press: Cambridge, U. K., 1993.
(26) Alexlson, D. E.; Russell, K. *Prog. Polym. Sci.* **1985**, *11*, 221−282.
(27) Zhang, X.; Do, M.; Hoobin, P.; Burgar, I. *Polymer* **2006**, *47*, 5888−5896.
(28) Zhang, X.; Hoobin, P.; Burgar, I.; Do, M. *Biomacromolecules* **2006**, *7*, 3466−3473.
(29) Zhang, X.; Hoobin, P.; Burgar, I.; Do, M. *J. Agric. Food Chem.* **2006**, *54*, 9858−9865.
(30) Chen, P.; Zhang, L.; Cao, F. *Macromol. Biosci.* **2005**, *5*, 872−880.

(31) Belton, P. S.; Duce, S.; Colquhoun, I. J.; Tatham, A. S. *Magn. Reson. Chem.* **1988**, *26*, 245−251.
(32) Belton, P. S.; Colquhoun, I. J.; Grant, A.; Weliner, N.; Field, J. M.; Shewry, P. R.; Tatham, A. S. *Int. J. Biol. Macromol.* **1995**, *17*, 74−80.
(33) Yoshimizu, H.; Ando, I. *Macromolecules* **1990**, *23*, 2908−2912.
(34) Terao, T.; Maeda. S.; Saika, A. *Macromolecules* **1983**, *16*, 1535−1539.
(35) Zhang, X.; Takegoshi, K.; Hikichi, K. *Polymer* **1992**, *33*, 722−728.
(36) Horii, F.; Masuda, K. ; Kaji, H. *Macromolecules* **1997**, *30*, 2519−2520.
(37) Masuda, K.; Kaji, H. ; Horii, F. *J. Polym. Sci., Part B: Polym. Phys.* **2000**, *38*, 1−9.
(38) Calucci, L.; Forte, C.; Galleschi, L.; Geppi. M.; Ghiringhelli, S. *Int. J. Biol. Macromol.* **2003**, *32*, 179−189.
(39) Belton, P. S.; Gil, A. M.; Grant, A.; Alberti, E.; Tatham, A. S. *Spectrochim. Acta, Part A* **1998**, *54*, 955−966.
(40) Alberti, E.; Gilbert, S. M.; Tatham, A. S.; Shewry, P. R.; Gil, A. M. *Biopolymer* **2001**, *58*, 33−45.
(41) Havenes, J. R.; VanderHart, D. L. *Macromolecules* **1985**, *18*, 1663−1676.
(42) Dickinson, L. C.; Yang, H.; Chu, C.-W.; Stein, R. S.; Chien, J. C. W. *Macromolecules* **1987**, *20*, 1757−1760.
(43) Zhang, X.; Takegoshi, K.; Hikichi, K. *Macromolecules* **1991**, *24*, 5756−5762.
(44) Zhang, X.; Takegoshi, K.; Hikichi, K. *Macromolecules* **1993**, *26*, 2198−2201.
(45) Zhang, X.; Solomon, D. H. *Macromolecules* **1994**, *27*, 4919−4926.

BM060929X